On-machine measurement of thermal influence of the long-span crossbeam of gantry machine tools using a 3D laser profiler

Zhiyang Zhao[a], Nuodi Huang[a]*, Lei Zhong[b], Zhengchun Du[a], Soichi Ibaraki[c], Limin Zhu[a]

a State Key Laboratory of Mechanical System and Vibration, School of Mechanical Engineering, Shanghai Jiao Tong University, Shanghai, 200240, China

b Shanghai Top Numerical Control Technology Co., Ltd.

c Graduate School of Advanced Science and Engineering, Hiroshima University, Kagamiyama 1-4-1, Higashi-Hiroshima, 739-8527, Japan

* Corresponding author, email: nhuang@sjtu.edu.cn

Abstract

For gantry machine tools, the large-span beam is an important structural component, and its deformation is significantly affected by temperature. It is still a crucial problem to identify the thermal error of the motion axis continuously and in real-time. This paper proposed an on-machine measurement (OMM) method to evaluate the thermal influence on long-span crossbeam of the gantry machine tools, using a high-precision 3D laser profiler and a set of artifacts. Firstly, kinematic model to compute the deformation of the crossbeam is established considering the position calibration of the laser profiler. As the Y-axis relies on the crossbeam, thermal errors of the Y-axis are identified to evaluate the thermal influence on long-span crossbeam. Secondly, algorithms for the position calibration and the point cloud registration are proposed to solve the calibration matrix and the relative transformation matrix of the 3D laser profiler in the kinematic model. The thermal error of the Y-axis can then be identified by utilizing the developed kinematic model. Finally, a continuous warm-up experiment was carried out on a three-axis gantry machine tool, and the six thermal errors of the Y-axes during the warm-up process were calculated. The results verify the effectiveness of the proposed method. In addition, uncertainty analysis is conducted to evaluate the effect of the 3D laser profiler calibration error on thermal error identification based on the experimental results. It is proved that the proposed thermal error identification method is insensitive to position calibration errors.

Keywords: Thermal error, long-span crossbeam, on-machine measurement, gantry machine tool, 3D laser profiler

1. Introduction

The accuracy of machine tools has a significant impact on machining accuracy, and is also a key indicator for evaluating the performance of the machine tools. Among the many error sources affecting the accuracy of machine tools, thermal error accounts for 40-70% of the total error [1], and up to 75% of the total geometric error of the machined workpiece is caused by the influence of temperature [2]. The thermal error of the machine tool is usually affected by the ambient temperature [3], the heat generated in the cutting process [4], and the heat generated by friction [5]. And the frictional heat is mainly generated by the drive unit for spindle rotation and movement of all the motion axes. The thermal error of the spindle is generally considered to be independent of the position of the spindle and is mainly influenced by the spindle speed [6], while the thermal error of the linear axis is not only related to the temperature of the linear axis, but also its coordinate position [7].

Large gantry machine tools have a large linear travel range, making it possible to machine large structural parts, such as large impeller blades, aircraft skins, bridge structures, etc. Due to their large volume and long axis travel range, the magnitude of the error source is amplified by the mechanical structure, compared to conventional-sized machine tools. For large gantry machines, reducing error sources through error avoidance or structural optimization is prohibitively expensive [8], while the error source reduction by compensation method is more cost-effective. Therefore, thermal error compensation methods are popular among scholars [9], and their identification and compensation are increasingly important to improve the accuracy of machine tools [10].

Measurement and identification of thermal error have always been a hot research topic as it is the basis of thermal error compensation. Due to the time variation and nonlinearity of thermal error, the measurement of short time shutdown will also lead to the change of thermal error, that is, the measurement of thermal error under static conditions is inaccurate. Therefore, it is necessary to measure the thermal error of large gantry machines quickly and accurately. The way to identify thermal errors can be divided into non-machining measurements and machining measurements. Displacement sensors are widely used for error measurement. Gomez-Acedo et al. [11] measured the thermal errors at different locations along three linear axes in the machine tool working volume using a reference artifact and eddy current sensors. Sato and Shirase [12] use laser displacement sensors for on-machine measurement of the machined artifact to identify geometric errors of the rotating axis of the five-axis machine tool. Abdulshahed et al. [13] measured the thermal displacement of the test bar using a laser displacement sensor and the thermal strain using fiber Bragg grating sensors. Ye et al. [14] used a laser interferometer to measure thermal positioning error and straightness error of gantry milling machine. Ibaraki et al. [15] measured the two-dimensional machining plane by tracking interferometer, which has the advantage of short measurement time. Later, Mori et al. [16] improved the method by identifying the position of the laser tracker, which greatly reduces the uncertainty and can be applied to machine tools without rotating axes. Ibaraki et al. [17] used a non-contact laser barrier to identify the influence of thermal error on the position error of the rotation axis. Non-machining test methods have a high measurement speed, which

can reduce downtime or even no downtime, but most of them measure positioning errors or motion trajectories. There are already commercially available 6-DOF laser measuring systems, such as the XM-60 by Renishaw. Such an instrument enables the measurement of six error motions at arbitrary points along a line. But its high instrumental cost can be an issue for practical implementation.

Machining tests are close to the actual machining environment and are another effective method to identify thermal error by measuring the geometry of the machined part. Liu et al. [18] designed a machining test method to observe the influence of thermal errors on the machining features of parts with the naked eye, but could not directly obtain the magnitude of thermal errors. Huang et al. [19] proposed a machining test method to visually identify the thermal error of a five-axis machine tool with the naked eye. Ibaraki and Okumura [20] proposed a machining test to evaluate the position and orientation errors of the thermal rotation axis mean lines. Wiessner et al. [21] designed a machining test to evaluate the thermal error of the rotary table machine tool, identifying the thermal error in the X-, Y-, and Z-directions and the two angular errors at the center point of the tool. Machining tests can identify numerous thermal errors, if designed properly. However, to measure over a long range, the workpiece should be as large as the measured travel. Limited by the volume and number of machined parts, measuring the linear axes of gantry machines with long-span crossbeams is time-consuming and expensive. Therefore, it is difficult to measure thermal errors for the large gantry machine tool.

Compared to these existing measurement schemes, the present scheme is an inexpensive and fast way to measure the thermal variation of six error motions of a linear axis at multiple positions throughout its travel. 3D laser profilers are often used for the inspection of part contours [22], or continuous inspection of roads and rails [23]. It has a high sampling rate and can obtain surface point cloud data of objects in a short time. In this paper, it is used to measure the six thermal errors of the Y-axis, which relies on the long-span crossbeam. First, the high-precision 3D laser profiler was installed at the end of the spindle and its position was calibrated. Then, an artifact was designed for the experiment, and a set of identical artifacts were placed on the bench at equal intervals, and the point cloud data of the artifact surface was obtained by the 3D laser profiler. Then, the thermal influence on the long-span crossbeam of gantry machine tools is quickly evaluated. By comparing with the first scanned point cloud, the laser profiler positional changes caused by heat are solved. Thereafter, the thermal error of the machine tool is captured for the whole process of the warm-up machine. A limitation of the present scheme is that it does not measure absolute values of the error motions at each measured location. It only measures their relative change from the initial value at each measured location. To measure absolute values of the error motions, the exact position and orientation of each artifact must be known in the machine coordinate system, which is in practice not possible. The remaining parts of the article are structured as follows. In Section 2, the OMM system model used in this paper is introduced. A linear axis thermal error model in the Y-direction of the gantry machining center was established so that the thermal error to be identified is represented by a homogeneous transformation matrix (HTM). In Section 3, an improved algorithm for 3D laser profiler position calibration is proposed based on the OMM system, and a method for solving the thermal error in the linear axis of the machine tool is given. In Section 4, the important parameters of the experimental setup including the artifacts are presented. What is more, the 3D laser profiler was calibrated for the position according to the method in the previous section, the thermal error of the Y-direction linear axis of the gantry machine tool was measured, and the experimental results were given. In Section 5, the influence of calibration error on measurement results is analyzed. In Section 6, the work and contributions of this paper are summarized.

2. On-machine measurement system setup

2.1. Machine tool configuration and thermal error to be identified

In this study, a three-axis gantry machining center is selected, as shown in Fig. 1. The slide installed on the beam is the Y-axis of the machine tool, and the ram installed on the slide is the Z-axis of the machine tool. Both move linearly along the guide rail.

To identify the thermal influence of long-span crossbeam, a 3D laser profiler based OMM system is utilized. The 3D laser profiler is installed on the spindle and measures the distance between the laser source and the surface of the object by receiving a high frequency reflected laser beam. The structure model and the kinematic chain of the OMM system are shown in Fig. 1. Note that the proposed method can be directly applied to the thermal error measurement of the linear axis for both three- and five-axis machine tools.

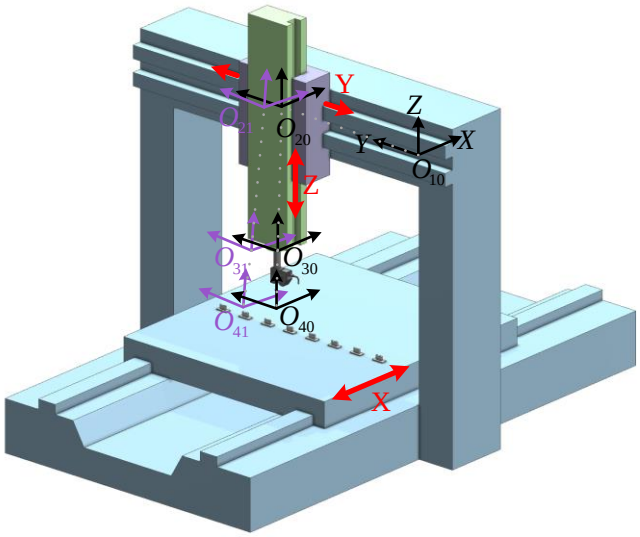

Fig. 1 3D laser profiler based on OMM system

The movement of the machine tool can be considered as combined motions of several rigid components. Local coordinate systems of each rigid body are established according to the machine tool structure and are set in the same direction as machine tool coordinate systems. As shown in Fig. 1, O_{10} represents the origin of the fixed local coordinate system at the limit of the Y-axis. O_{20} represents the origin of the slide coordinate system containing geometric errors, whose position is determined by the CNC system of the machine tool and the geometric error items. O_{21} represents the origin of the slide coordinate system containing geometric and thermal errors (similarly hereinafter). O_{30} represents the origin of the tool coordinate system (TCS) containing the geometric error. O_{40} represents the origin of the 3D laser profiler coordinate system (LCS) containing geometric error.

The six geometric and thermal errors associated with Y-axis are shown in Table 1, whose definitions are given by ISO 230-1 [24] and ISO 230-3 [25], respectively.

Table 1 Geometric and thermal errors associated with Y-axis

Geometric errors associated with Y-axis		Thermal errors associated with Y-axis	
Symbol	Description	Symbol	Description
δ_{xy}	Straightness error in X-axis direction	δ'_{xy}	Thermal straightness error in X-axis direction
δ_{yy}	Linear positioning error of Y-axis	δ'_{yy}	Thermal linear positioning error of Y-axis
δ_{zy}	Straightness error in Z-axis direction	δ'_{zy}	Thermal straightness error in Z-axis direction
ε_{xy}	Angular error around X-axis (pitch)	ε'_{xy}	Thermal angular error around X-axis (pitch)
ε_{yy}	Angular error around Y-axis (roll)	ε'_{yy}	Thermal angular error around Y-axis (roll)
ε_{zy}	Angular error around Z-axis (yaw)	ε'_{zy}	Thermal angular error around Z-axis (yaw)

Since the geometric or thermal errors are only tens of micrometers or thousandths of a degree, higher-order terms are neglected during kinematic modeling.

2.2. Kinematic modeling of the linear axis including geometric and thermal errors

Due to the gantry structure and working environment, the thermal effect significantly affects the crossbeam deflection. A kinematic model is established to quickly evaluate the thermal influence on the long-span crossbeam of gantry machine tools. To prevent interference from other axes errors, keep the other translational axes fixed. The machine tool is started from the cold state and only geometric error is considered. Then the HTM of the local coordinate system O_{40} to O_{10} is expressed as

$$
\begin{aligned}
{}^{O_{10}}_{O_{40}}T &= {}^{O_{10}}_{O_{20}}T \cdot {}^{O_{20}}_{O_{30}}T \cdot {}^{O_{30}}_{O_{40}}T \\
&= \begin{bmatrix} 1 & -\varepsilon_{zy} & \varepsilon_{yy} & \delta_{xy} \\ \varepsilon_{zy} & 1 & -\varepsilon_{xy} & y+\delta_{yy} \\ -\varepsilon_{yy} & \varepsilon_{xy} & 1 & \delta_{zy} \\ 0 & 0 & 0 & 1 \end{bmatrix} \begin{bmatrix} 1 & 0 & 0 & x_y \\ 0 & 1 & 0 & 0 \\ 0 & 0 & 1 & z_y \\ 0 & 0 & 0 & 1 \end{bmatrix} \begin{bmatrix} a_{11} & a_{12} & a_{13} & b_{11} \\ a_{21} & a_{22} & a_{23} & b_{21} \\ a_{31} & a_{32} & a_{33} & b_{31} \\ 0 & 0 & 0 & 1 \end{bmatrix}
\end{aligned} \tag{1}
$$

where y denotes the Y-axis position. x_y and z_y represent the distances along the X-axis and Z-axis from the Y-axis lead

screw, respectively, and are fixed distances. $a_{11} \sim a_{33}$, $b_{11} \sim b_{31}$ denote the attitude and position changes of the LCS relative to the TCS, i.e., the matrix ${}^{O_{30}}_{O_{40}}T$.

During the warm-up process or when the ambient temperature changes, thermal errors exist and are accumulated gradually. The HTM of the local coordinate system O_{21} to O_{20} is expressed as

$$ {}^{O_{20}}_{O_{21}}T = \begin{bmatrix} 1 & -\varepsilon'_{zy} & \varepsilon'_{yy} & \delta'_{xy} \\ \varepsilon'_{zy} & 1 & -\varepsilon'_{xy} & \delta'_{yy} \\ -\varepsilon'_{yy} & \varepsilon'_{xy} & 1 & \delta'_{zy} \\ 0 & 0 & 0 & 1 \end{bmatrix} \tag{2} $$

According to Eq. (1) and Eq. (2), the HTM of the coordinate system O_{21} to O_{20} can be expressed by another transformation processes

$$ \begin{aligned} {}^{O_{20}}_{O_{21}}T &= {}^{O_{20}}_{O_{30}}T \cdot {}^{O_{30}}_{O_{40}}T \cdot {}^{O_{40}}_{O_{41}}T \cdot {}^{O_{41}}_{O_{31}}T \cdot {}^{O_{31}}_{O_{21}}T \\ &= {}^{O_{20}}_{O_{30}}T \cdot {}^{O_{30}}_{O_{40}}T \cdot \begin{bmatrix} R & T \\ 0 & 1 \end{bmatrix} \cdot {}^{O_{30}}_{O_{40}}T^{-1} \cdot {}^{O_{20}}_{O_{30}}T^{-1} \end{aligned} \tag{3} $$

where ${}^{O_{40}}_{O_{41}}T$ denotes the HTM of the 3D laser profiler LCS in the cold and warm state of the gantry machine, which contains the 3×3 rotation matrix R and the 3×1 translation vector T. Eq. (3) is another expression of HTM ${}^{O_{20}}_{O_{21}}T$, which contains all the thermal error terms of the linear axis. According to the form of Eq. (3), it contains two unknown HTMs ${}^{O_{30}}_{O_{40}}T$ and ${}^{O_{40}}_{O_{41}}T$. Therefore, the thermal error of the linear axis can be obtained by identifying two unknown HTMs, and their identifying algorithms will be introduced in the next section.

3. Identification of thermal error

3.1. OMM based thermal error identification procedure

The thermal error identification procedure is divided into two parts. Firstly, the position calibration of the 3D laser profiler installed at the end of the spindle is calibrated by means of the processing program and the scanning of the 3D laser profiler, and the HTM from the LCS to the TCS is obtained. Secondly, the 3D laser profiler is used to scan artifacts, and to register the point cloud data obtained in the cold state and warm state to obtain the position and attitude changes of the 3D laser profiler. The laser profiler position calibration algorithm is used to determine the transformation relationship of local coordinate system O_{40} to O_{30}, ${}^{O_{30}}_{O_{40}}T$. The point cloud registration algorithm is used to identify the relative change of the LCS of the laser profiler, ${}^{O_{40}}_{O_{41}}T$.

In the 3D laser profiler position calibration process, a circular pocket is machined by the machine tool, as shown in Fig. 2. The accuracy center position and radius of the circular pocket in the TCS are obtained. The 3D laser profiler is then installed on the spindle to capture the geometry of the circular pocket. By comparing the designed and reconstructed center position and radius of the circular pocket, the HTM of two coordinate systems O_{40} to O_{30} is solved based on curve fitting of least square method. The detailed algorithm will be introduced in Section 3.2. To prevent unwanted laser scanning errors, the 3D laser profiler should not be disassembled or adjusted after completing the position calibration operation.

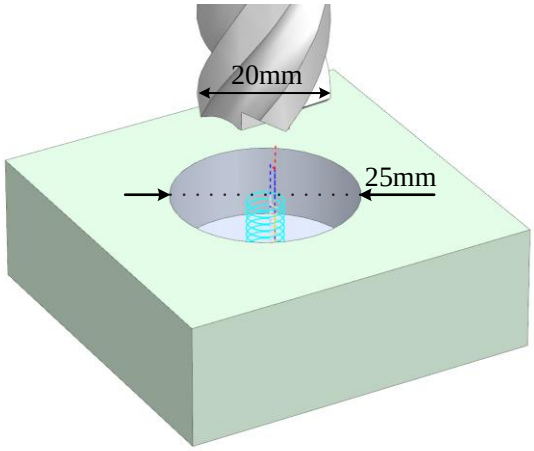

Fig. 2 Designed part with circular geometric features

Once the position calibration process is complete, a warm-up program is designed to allow the 3D laser profiler to scan the artifacts, which are placed at equal intervals on the machine workbench. By registering the point cloud data obtained during the cold state and warm-up process of the machine tool, the position and attitude changes of the 3D laser profiler LCS

caused by the thermals are obtained. Then obtain the thermal error of different warm-up times and corresponding position of the machine tool according to Eq. (3). The detailed algorithm will be introduced in Section 3.3.

The 3D laser profiler measures distance based on the laser triangulation principle, where the laser light is incident vertically and reflected onto the light-sensitive element. Therefore, it is necessary to prevent the reflected light from being blocked by the artifact which means that the maximum inclination of the surface in the Y-direction does not exceed the specified value, which depends on the parameters of the 3D laser profiler. It should be noted that the triangulation-based laser sensor may be subject to measurement noise. Therefore, this study uses a large number of filtered point cloud registration and data fitting methods to process data to reduce noise interference. The measurement repeatability of the 3D laser profiler should be as high as possible. The Z direction repeatability accuracy of the 3D laser profiler used in this study is 0.5 μm, which meets the experimental requirements. More parameters will be introduced in Section 4.1. An artifact with a free-form surface is designed and used as the measurement object, as shown in Fig. 3. The equation of the free-form surface is as follows. The curves of the X-Z plane are taken as section curves and Y-Z plane curves are taken as guide curves. Surfaces are generated by sweeping. The top surface design of the artifact is not unique, but changes in measurement data should be reflected as sensitive as possible by changes in thermal error. Therefore, the top surface should be designed with an inclination angle that does not exceed the maximum specified value for a 3D laser profiler. The experiment uses a comparative method to identify thermal errors, so there is no special requirement for the precision of the artifact. However, there should be no surface defects on the measured surface of the artifact. It is possible to manufacture the artifacts using metalworking or 3D printing.

$$\begin{cases} z_x = \sin(\frac{3}{5}x), x \in [0,11] \\ z_y = \frac{5}{2}\sin(\frac{1}{6}y), y \in [0,41] \end{cases} \tag{4}$$

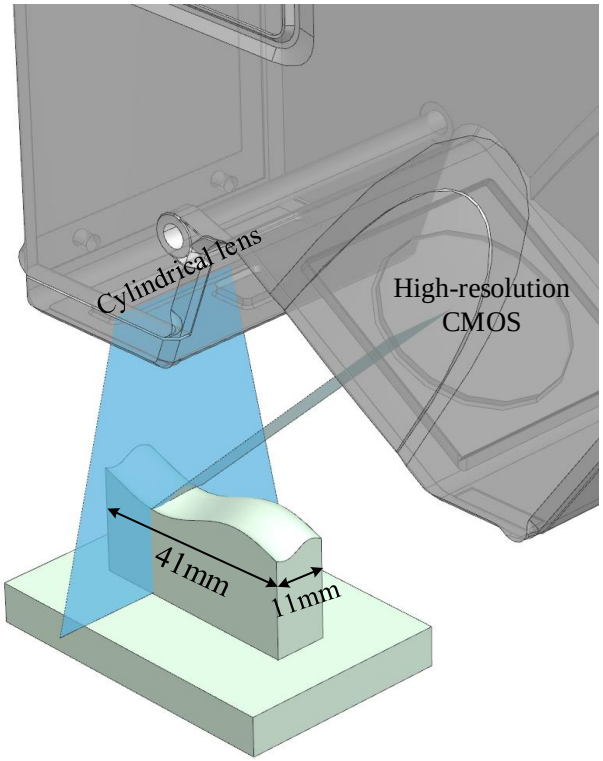

Fig. 3 Artifact model with free surface and measurement schematic

3.2. 3D laser profiler position calibration

Due to the installation errors and the volume of the 3D laser profiler itself, the LCS of the 3D laser profiler does not coincide with the TCS which affects the accuracy of the thermal error solution. If the installer is experienced, the impact of installation errors can be neglected. Otherwise, it is necessary to conduct a calibration process to calibrate the deviation between TCS and LCS. This section improves the calibration method proposed in reference [26], which can identify not only the installation displacement error but also the installation angle error. In the TCS, the center coordinates and radius of the machined circular pocket are represented by (X_0, Y_0, Z_0, r). The coordinate data of the circular pocket edge in the LCS can be obtained by the 3D laser profiler.

According to rigid body kinematics, when a rigid body changes its position and orientation in space, its HTM can be expressed as

$$T = T_X(\Delta x) \cdot T_Y(\Delta y) \cdot T_Z(\Delta z) \cdot R_X(\alpha) \cdot R_Y(\beta) \cdot R_Z(\gamma) \tag{5}$$

where $T_X(\Delta x)$, $T_Y(\Delta y)$, and $T_Z(\Delta z) \in \mathbb{R}^{4\times4}$ represent the HTM for linear motion of values Δx, Δy and Δz in X-, Y-, and Z-directions, respectively. $R_X(\alpha)$, $R_Y(\beta)$, and $R_Z(\gamma) \in \mathbb{R}^{4\times4}$ represent the HTM for angular motion of values α, β, and γ around the X-, Y-, and Z-axes, respectively.

According to Eq. (5), the transformation matrix between the LCS and the TCS ${}^{O_{30}}_{O_{40}}T$ can be solved by identifying six parameters α, β, γ, Δx, Δy and Δz, as shown in Eq. (6).

$$ {}^{O_{30}}_{O_{40}}T = \begin{bmatrix} C\beta C\gamma & -C\beta S\gamma & S\beta & \Delta x \\ C\alpha S\gamma + C\gamma S\alpha S\beta & C\alpha C\gamma - S\alpha S\beta S\gamma & -C\beta S\alpha & \Delta y \\ S\alpha S\gamma - C\alpha C\gamma S\beta & C\gamma S\alpha + C\alpha S\beta S\gamma & C\alpha C\beta & \Delta z \\ 0 & 0 & 0 & 1 \end{bmatrix} \tag{6} $$

where S and C are shorthand for sine and cosine functions, respectively. Note that the angular error β causes the scanned plane profile to tilt, and the tilt angle also equals to β. Thus, the angular error β can be identified by calculating the tilt angle of the scanned plane profile using linear least squares fitting method. During the calibration process, the machine tool moves in the positive direction along the Y-axis to scan the circular pocket. The circular contour can be obtained by extracting the edge features of the scanning contour. The coordinates of the circular contour points in the TCS are: $P_{O_{30}} = [X_p \quad Y_p \quad Z_p]^T$, and the coordinates in the LCS are $P_{O_{40}} = [(i-1600)\Delta d \quad Y_L \quad Z_L]^T$, where i represents the *i-th* measuring point of each laser profile, half of the X-direction profile data count is 1600, Δd represents profile data interval (12.5 μm). As a result, the coordinate conversion relationship between the TCS and the LCS is shown in Eq. (7).

$$ P_{O_{30}} = {}^{O_{30}}_{O_{40}}T \cdot P_{O_{40}} = {}^{O_{30}}_{O_{40}}T \cdot \begin{bmatrix} (i-1600)\Delta d \\ Y_L \\ Z_L \\ 1 \end{bmatrix} \tag{7} $$

In the TCS, the coordinates of the circle contour point all satisfy the following equation

$$ \begin{cases} (X_p - X_0)^2 + (Y_p - Y_0)^2 = r^2 \\ Z_p = Z_0 \end{cases} \tag{8} $$

According to Eq. (7), the circle contour coordinates in the LCS are transformed to the TCS, and the transformed circle contour coordinates all satisfy Eq. (8). Note that the above conversion process contains five unknown parameters, which can be solved by the nonlinear curve fitting based on least-squares method [27]. The form of nonlinear curve fitting function based on least square method is as follows

$$ \min_{\lambda} \left\| F(\lambda, \lambda_{data}) - y_{data} \right\|_2^2 = \min_{\lambda} \sum_i \left(F(\lambda, \lambda_{data_i}) - y_{data_i} \right)^2 \tag{9} $$

where λ is the five unknown parameters α, γ, Δx, Δy and Δz that still need to be identified, λ_{data} is the input data $P_{O_{40}}$ of Eq. (7), and y_{data} is the observable value in Eq. (8).

3.3. Thermal error calculation based on relative position transformation

The position of the spindle related to the artifact is significantly influenced by the thermal error. Thus, it is necessary to obtain the change of the spindle end position at the same position in the Y-direction at each warm-up cycle. In general, it is difficult to directly measure the posture of the end of the spindle in real-time when the machine tool is moving continuously. This section presents a new method to directly measure the position of the spindle in real-time, by using a 3D laser profiler. The point cloud coordinates of the tested parts are obtained in real-time by using the 3D laser profiler. During the measurement, it is necessary to ensure that the position of each artifact does not change. By registering the point cloud data measured at different warming-up cycles, the relative change of the spindle end position can be obtained. The thermal error of the machine tool can be solved according to Eq. (3).

The Iterative Closest Point (ICP) algorithm is used to register each group of point cloud data, and the rotation matrix R and translation vector t used for its process are obtained [28]. Parameters R and t can be determined by minimizing the Euclidean distance between the source and the target point clouds through the ICP algorithm, whose equation is shown as follows.

$$ f(R,t) = \arg\min \frac{1}{n} \sum_{i=1}^{n} \left\| (Rp_i + t) - q_i \right\|^2 \tag{10} $$

where p_i represents the point in the source point cloud; q_i represents the point cloud measured in the cold state; $i \in [1, 2, \cdots, n]$, and n represents the total number of points in the target point cloud. The parameters R and t obtained by the ICP algorithm are substituted into the HTM ${}^{O_{40}}_{O_{41}}T$, and then six thermal errors of the linear axis can be solved by Eq. (3).

Since the ICP registration algorithm is sensitive to the initial values, noise, and outliers of the point cloud data, it is only suitable for the final precision registration process. The point cloud data scanned by the 3D laser profiler contains noise. Some outliers are present in the point cloud data of the artifact edge contours. These relate to stray light and ambient light when reflected. Therefore, pre-processing and pre-registration must be involved to increase the accuracy of point cloud registration. First, the edge contour of the artefact is identified according to the point cloud data, and 20 consecutive data points (250μm) near the edge contour are removed in order to completely remove the edge outliers. Then, a statistical-based filtering method is used to remove the noise value by calculating the average μ and standard deviation σ of the nearest neighbor distance [29]. The above is the strategy for removing noisy points and outliers. After removing noisy points and outliers, the pre-registration for proper initial value determination is developed. The Normal Distribution Transform (NDT) registration algorithm is a widely used coarse registration algorithm. Compared with the ICP algorithm, the NDT algorithm converges from a larger range of initial position estimation [30]. Therefore, the NDT algorithm is used for pre-registration and the registration result is taken as the initial transformation of ICP registration. Finally, all six thermal errors of linear axis of gantry machine are identified by using the NDT-ICP algorithm.

4. Experiments

4.1. Experimental setup

The selected three-axis gantry machine tool has a travel range of $X \times Y \times Z = 4 \times 1.8 \times 1$ m. The 3D laser profiler Keyence LJ-X8080 is installed at the end of the spindle with a tool shank and an aluminum metal bracket. The point cloud data on the surface of the artifact and the position of the machine tool are obtained by the 3D laser profiler and CNC system. The important specifications of the 3D laser profiler are listed in Table 2.

Table 2 Important specifications of 3D laser profiler [31]

Specifications	Z-direction (Height)	X-direction (width)	Y-direction (scan)
Reference distance	73 mm		
Measurement range	±20.5 mm (F.S.=41 mm)	35 mm	
Repeatability	0.5 μm	1 μm	
Linearity	±0.03% of F.S.		
Profile data count		3200 data	60000 (max)
Profile data interval		10~12.5 μm	
Sampling period			1 kHz (Full range)

4.2. Position calibration of 3D laser profiler

Before the calibration experiment starts, the necessary preparations are as follows: the milling cutter is installed at the end of the spindle and the spindle of the machine tool is moved over the workbench by the CNC system. Next, an epoxy board is placed on the workbench under the spindle as the blank to be machined, as shown in Fig. 4(a). According to the pre-designed NC code, a circular pocket is machined on the epoxy tooling board. Record the data of the circular pocket in the tool coordinate system, where the radius is measured with a micrometer, that is $(X_0, Y_0, Z_0, r) = (0, 0, 0, 12.496)$. The calibration experiment is conducted according to the method described in Section 3.1. The process of scanning the circular pocket with a 3D laser profiler after machining is shown in Fig. 4(b). To minimize the calibration error, a dial indicator is used to make the X-axis of the laser sensor parallel to the X-axis of the machine tool as much as possible.

The value of the β is identified firstly. The least squares fitting method is used to fit 3000 data points of plane scanning. A total of 80 sets of data were fitted and the average inclination angle $\beta = -0.0013$ rad was obtained from the tilt angle of the line. The solution process of the angle β is shown in Fig. 5, where the vertical axis scale is enlarged 20 times. The coordinates of the extracted edge points are substituted into Eq. (7) and the coordinates containing the unknown parameters are substituted into Eq. (8) for nonlinear least squares fitting. The calibration results of the remaining 5 parameters are as follows: $\alpha = 0.0029$ rad, $\gamma = -0.0091$ rad, $\Delta x = 2.771$ mm, $\Delta y = -0.876$ mm, and $\Delta z = 4.219$ mm. The HTM ${}^{O_{30}}_{O_{40}}T$ is obtained from the calibration results and the Z-axis lifting height of 178.152 mm when installing the 3D laser profiler, as shown in Eq. (11). The nonlinear curve fitting result based on the least square method is shown in Fig. 6.

$$ {}^{O_{30}}_{O_{40}}T = \begin{bmatrix} 0.9999579 & 0.0090741 & -0.001301 & 2.7710384 \\ -0.009074 & 0.9999546 & -0.002897 & -0.876047 \\ 0.0012751 & 0.0028967 & 0.9999949 & -173.9324 \\ 0 & 0 & 0 & 1 \end{bmatrix} \tag{11} $$

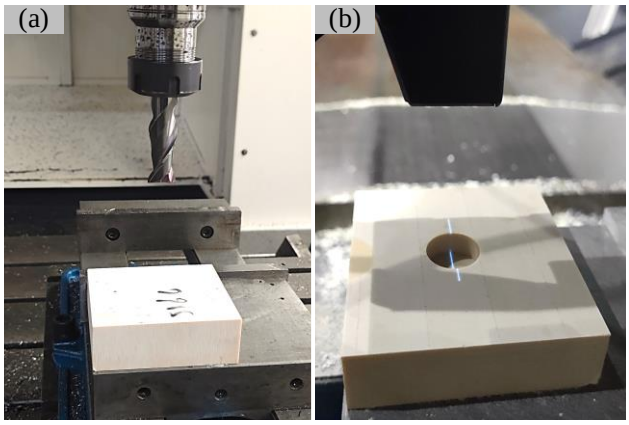

Fig. 4 The process of machining and calibration: (a) Epoxy plate machining, (b) 3D laser profiler scanning

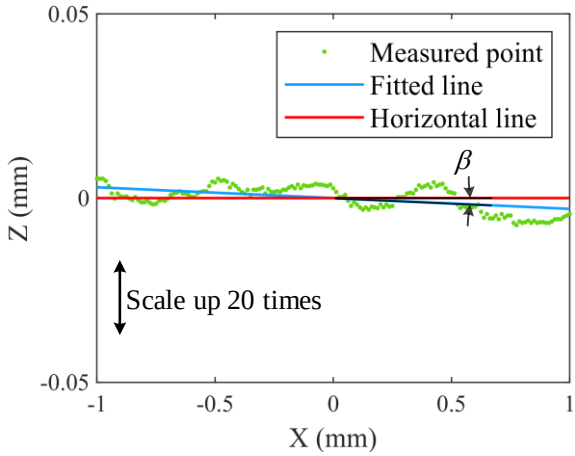

Fig. 5 Fitting β using the least squares method

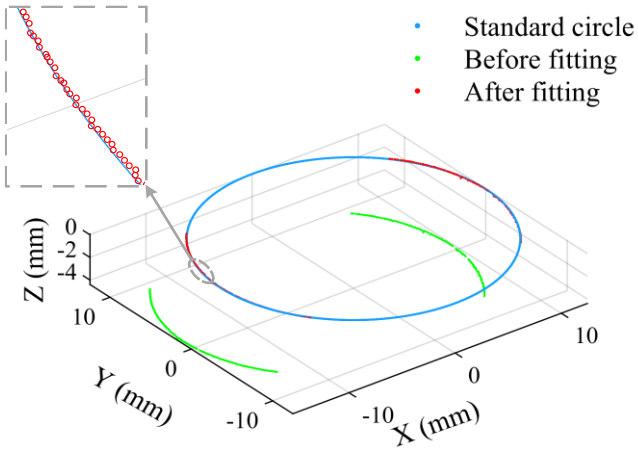

Fig. 6 Fitting circles with least squares to identify parameters

4.3. Error measurement of the linear axis

After completing the calibration experiment, the artifacts are placed on the worktable along the Y-direction. In this work, the artifacts are placed at an interval of 200 mm, and the first artifact is 350 mm away from the origin of the machine tool Y-direction. Eight artifacts are placed on the machine workbench, and the thermal error measurement range is 0~1750 mm. Moving the spindle position enables the 3D laser profiler to scan the artifacts completely and record the position of the end of the spindle in the CNC system. And measure the distance between the origin of the TCS and the Y-axis ball screw in the X and Z-directions, that is, $x_y = -900$ mm, $z_y = -2051$ mm in the transfer matrix ${}^{O_{20}}_{O_{30}}T$.

During the warm-up process, only the Y axis of the gantry machining center is moved, and the machine tool spindle is reciprocated in the Y-direction through the CNC system. The feed rate for the warm-up process is set to 3600 mm/min, and the feed rate for the measurement process is set to 1500 mm/min. The placement and scanning process of artifacts are shown in Fig. 7. Fig. 7 shows the setup of the 3D laser profiler. The aluminum metal bracket is installed on the tool holder and screwed to the 3D laser profiler. The installation of 3D laser profiler and tool handle was completed in the preparation of the experiment. In the experiment, the 3D laser profiler is installed on the machine tool by replacing the tool handle without

detaching the milling cutter. The machine warm-up process lasted 180 min and was measured 9 times at 7 min, 15 min, 30 min, 45 min, 60 min, 90 min, 120 min, 150 min, and 180 min after the start of the warm-up. At the beginning of the hot engine process, the temperature of the machine tool rises rapidly, so the measurement interval within the first 60 min is short. The point cloud (one of them) obtained by scanning the artifact before the machine tool is warmed-up is shown in Fig. 8. The schematic diagram of the NDT-ICP registration process of the point cloud is shown in Fig. 9. The target point cloud is relatively sparse, and the edges are processed, and the source point cloud is denser and displayed transparently in the figure. The 3D laser profiler takes about 1 hour to set up and position calibration, and the machine warm-up lasts 3 hours. The whole experiment was completed within 5 hours.

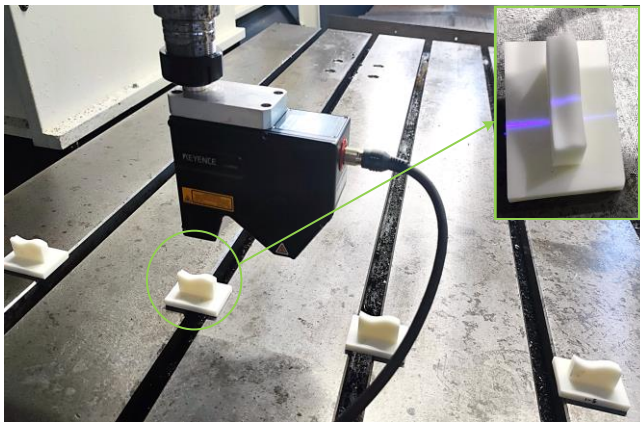

Fig. 7 3D laser profiler scanning

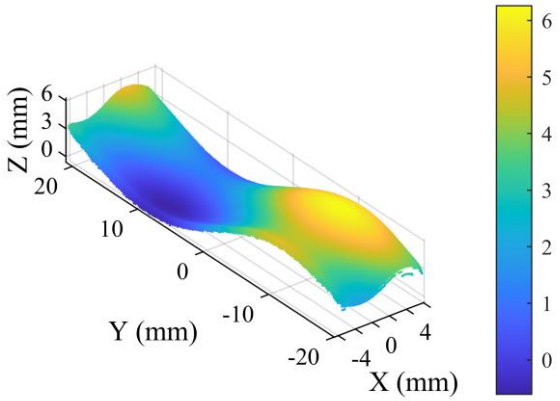

Fig. 8 Point cloud data obtained by cold scanning

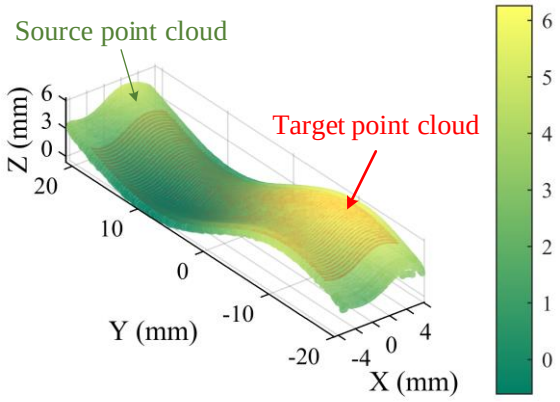

Fig. 9 Point cloud after NDT-ICP registration

4.4. Thermal error measurement results

By scanning the acquired point cloud data and the point cloud registration process described in Section 3.3, six thermal errors about the Y-axis are obtained. The registration accuracy is evaluated by the root mean square error (RMSE) of the Euclidean distance between the inlier aligned points. The average value of RMSE is 0.021 and the minimum value is 0.007. The thermal positioning error δ'_{yy} is shown in Fig. 10(a), and the thermal straightness error δ'_{xy} and δ'_{zy} are shown in Fig. 10(b) and Fig. 10(c), respectively. The thermal pitch error ε'_{xy}, roll error ε'_{yy}, and yaw error ε'_{zy} are shown in Fig. 11(a),

Fig. 11(b), and Fig. 11(c) respectively. The x-axis of the figure represents the different positions along the Y-axis of the machine, the y-axis represents the different warm-up times, and the z-axis represents the varying thermal errors.

According to the 6 sets of experimental results in Fig. 10 and Fig. 11, the thermal error of the machine tool changes significantly within 30 minutes after the machine is warmed-up, the Y-axis is close to thermal equilibrium when the machine is warmed-up for 150 minutes, and the thermal error fluctuation range is small in two adjacent periods of time. The thermal positioning error of the machine is most significantly affected by temperature and increases along the positive direction of the Y-axis as the warm-up time increases. The change of straightness error in the X and Z-directions is small, the thermal error in the X-direction fluctuates greatly at different positions, and the thermal error in the Z-direction has a trend of increasing first and then decreasing, which may be related to the geometric error of the machine tool itself. The thermal pitch error $\varepsilon_{xy}^{'}$ decreases with the increase of the warm-up time, and decreases with the increase of the position, but has an increasing trend around 1150 mm, but the increasing trend is not obvious. The trend of the thermal roll error is stable and increases with the increase of the warm-up time and position. The thermal yaw error decreases with the increase of position, and the warm-up time change has no obvious effect on the error.

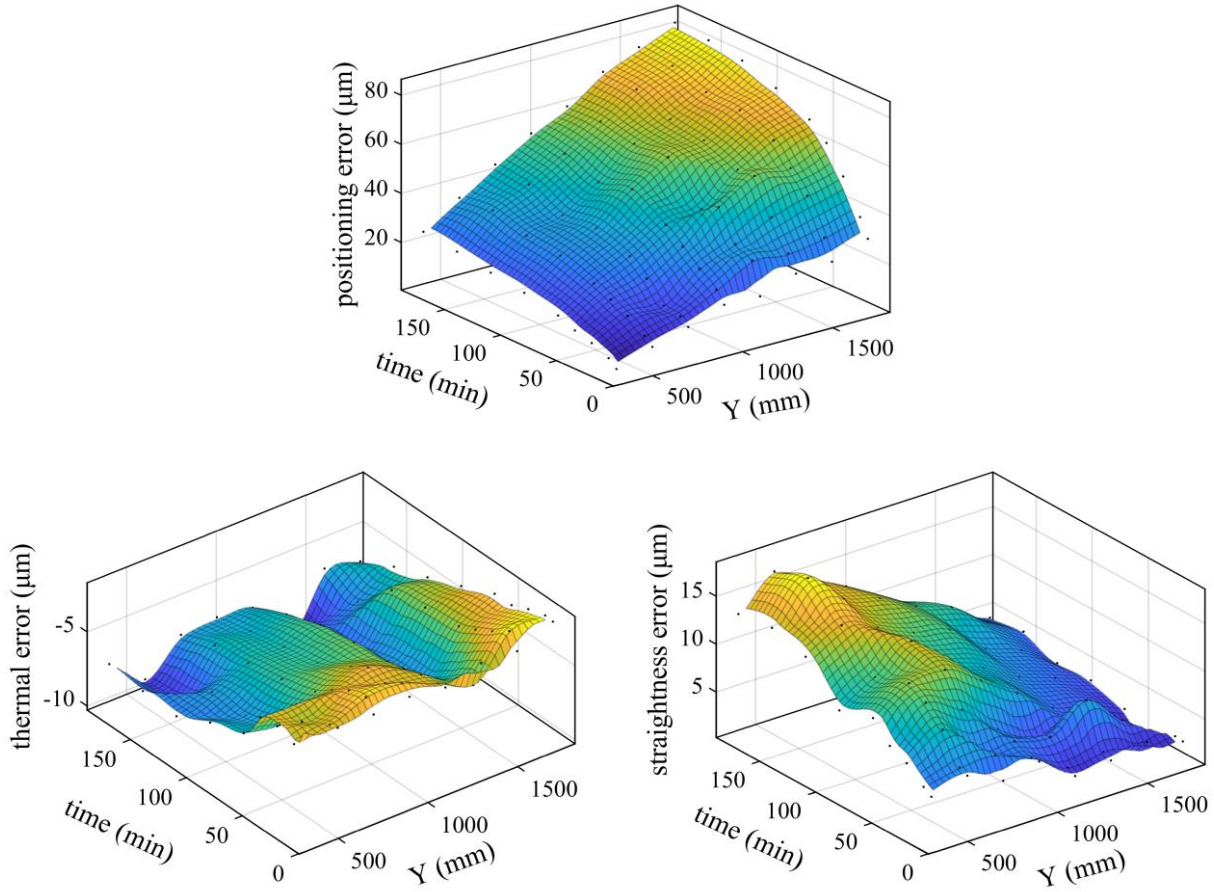

Fig. 10 Displacement error: (a) thermal positioning error $\delta_{yy}^{'}$, (b) X-direction thermal straightness error $\delta_{xy}^{'}$, (c) Z-direction thermal straightness error $\delta_{zy}^{'}$

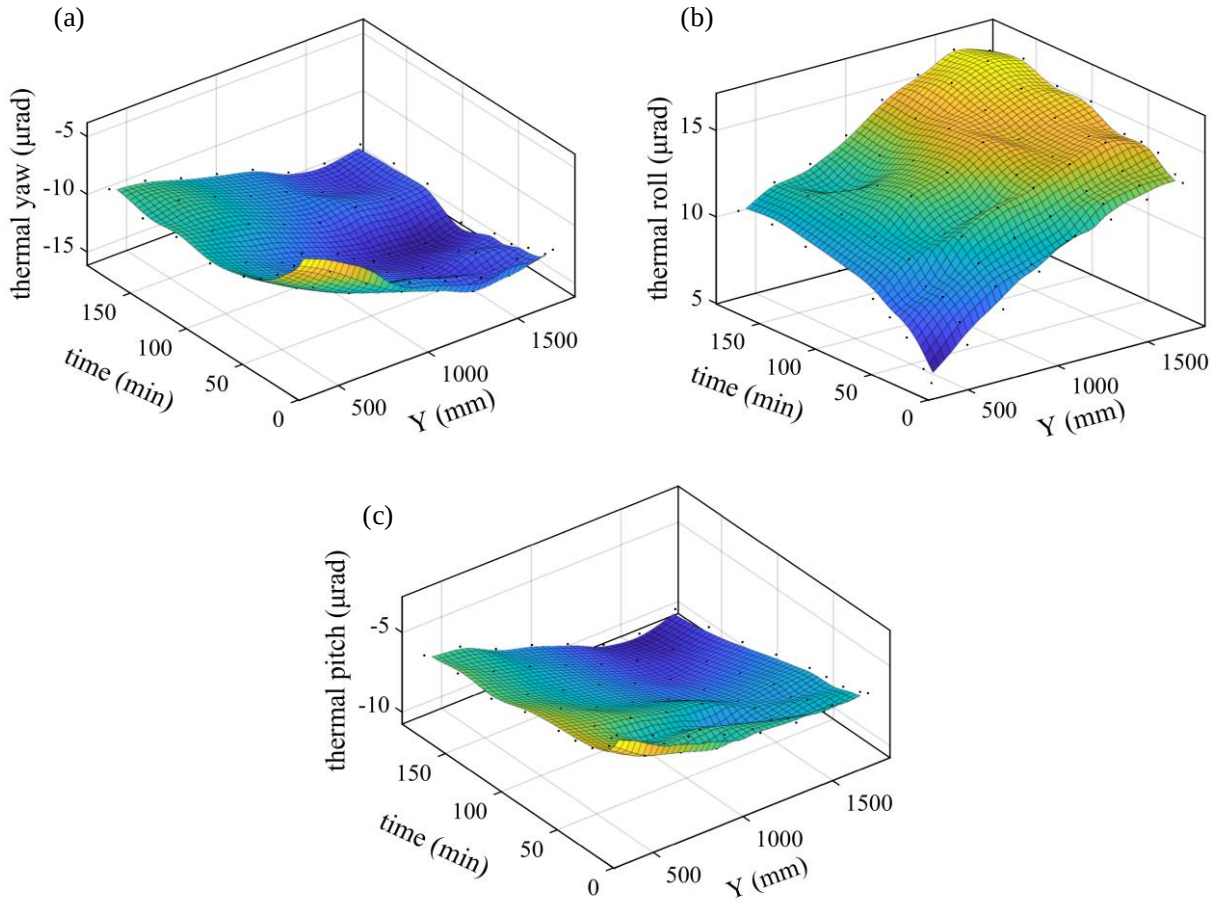

Fig. 11 Angle error: (a) thermal pitch error ε'_{xy}, (b) thermal roll error ε'_{yy}, (c) thermal yaw error ε'_{zy}

5. Position calibration error analysis of 3D laser profiler

Discontinuity of the point cloud data and the accuracy of the circular pocket processing make the calibration error unavoidable, so it is necessary to analyze the calibration errors. The derivation in this section aims to show that the error generated by the calibration process has little effect on the solution of the thermal error. The thermal error calculated using the calibration method in section 3.1 is denoted as ${}^{O_{20}}_{O_{21}}T_c$, and the true value is recorded as ${}^{O_{20}}_{O_{21}}T_t$.

$$
{}^{O_{20}}_{O_{21}}T_c = \begin{bmatrix} 1 & 0 & 0 & x_y \\ 0 & 1 & 0 & 0 \\ 0 & 0 & 1 & z_y \\ 0 & 0 & 0 & 1 \end{bmatrix} \begin{bmatrix} 1 & -\gamma & \beta & a \\ \gamma & 1 & -\alpha & b \\ -\beta & \alpha & 1 & c \\ 0 & 0 & 0 & 1 \end{bmatrix} \begin{bmatrix} 1 & -\psi & \varphi & \delta_x \\ \psi & 1 & -\omega & \delta_y \\ -\varphi & \omega & 1 & \delta_z \\ 0 & 0 & 0 & 1 \end{bmatrix} \begin{bmatrix} 1 & -\gamma & \beta & a \\ \gamma & 1 & -\alpha & b \\ -\beta & \alpha & 1 & c \\ 0 & 0 & 0 & 1 \end{bmatrix}^{-1} \begin{bmatrix} 1 & 0 & 0 & x_y \\ 0 & 1 & 0 & 0 \\ 0 & 0 & 1 & z_y \\ 0 & 0 & 0 & 1 \end{bmatrix}^{-1} \tag{12}
$$

$$
\begin{aligned}
{}^{O_{20}}_{O_{21}}T_t = &\begin{bmatrix} 1 & 0 & 0 & x_y \\ 0 & 1 & 0 & 0 \\ 0 & 0 & 1 & z_y \\ 0 & 0 & 0 & 1 \end{bmatrix} \begin{bmatrix} 1 & -\gamma-\Delta\gamma & \beta+\Delta\beta & a+\Delta a \\ \gamma+\Delta\gamma & 1 & -\alpha-\Delta\alpha & b+\Delta b \\ -\beta-\Delta\beta & \alpha+\Delta\alpha & 1 & c+\Delta c \\ 0 & 0 & 0 & 1 \end{bmatrix} \begin{bmatrix} 1 & -\psi & \varphi & \delta_x \\ \psi & 1 & -\omega & \delta_y \\ -\varphi & \omega & 1 & \delta_z \\ 0 & 0 & 0 & 1 \end{bmatrix} \\
&\begin{bmatrix} 1 & -\gamma-\Delta\gamma & \beta+\Delta\beta & a+\Delta a \\ \gamma+\Delta\gamma & 1 & -\alpha-\Delta\alpha & b+\Delta b \\ -\beta-\Delta\beta & \alpha+\Delta\alpha & 1 & c+\Delta c \\ 0 & 0 & 0 & 1 \end{bmatrix}^{-1} \begin{bmatrix} 1 & 0 & 0 & x_y \\ 0 & 1 & 0 & 0 \\ 0 & 0 & 1 & z_y \\ 0 & 0 & 0 & 1 \end{bmatrix}^{-1}
\end{aligned} \tag{13}
$$

where the true value is defined as $\alpha+\Delta\alpha$, $\beta+\Delta\beta$, $\gamma+\Delta\gamma$, $a+\Delta a$, $b+\Delta b$ and $c+\Delta c$, respectively. Rotation angle and displacement in the HTM ${}^{O_{40}}_{O_{41}}T$ are represented by ω, φ, ψ, δ_x, δ_y and δ_z, respectively. Then the error due to $\Delta*$ is expressed as

$$
{}^{O_{20}}_{O_{21}}T_c - {}^{O_{20}}_{O_{21}}T_t = \begin{bmatrix} \Delta R & \Delta T \\ 0 & 1 \end{bmatrix}
$$

$$
\Delta R = \begin{bmatrix} 0 & \omega\Delta\beta + \varphi\Delta\alpha & \omega\Delta\gamma - \psi\Delta\alpha \\ -\omega\Delta\beta + \varphi\Delta\alpha & 0 & -\psi\Delta\beta + \varphi\Delta\gamma \\ \psi\Delta\alpha - \omega\Delta\gamma & \psi\Delta\beta - \varphi\Delta\gamma & 0 \end{bmatrix} \tag{14}
$$

$$
\Delta T = \begin{bmatrix} \delta_z\Delta\beta - \delta_y\Delta\gamma + \psi\Delta b - \varphi\Delta c \\ \delta_x\Delta\gamma - \delta_z\Delta\alpha + \omega\Delta c - \psi\Delta a \\ \delta_y\Delta\alpha - \delta_x\Delta\beta - \omega\Delta b + \varphi\Delta a \end{bmatrix}
$$

Eq. (14) shows that the effect of calibration errors on the measurement results is the product of calibration error and machine tool error. According to the calibration results, the magnitude of the calibration angle error is between 0.01 rad and 0.001 rad, and the magnitude of the displacement error is between 1 mm and 0.1 mm. According to the error characteristics of the gantry machine tool, the magnitude of the angle error is 10^{-5} rad and the displacement is about 0.01 mm. The angle error caused by the calibration error is on the order of 10^{-7} rad and the displacement error is on the order of 0.1 μm. It shows that the thermal error solution method by comparing the relative changes of point cloud data does not require high calibration accuracy.

6. Conclusions

This paper presents a method for OMM of thermal errors on the long-span crossbeam of gantry machining tools. The 3D laser profiler is used to construct the OMM system, which can measure the thermal errors without stopping the machine tool during the test process. Considering the installation deviation of the 3D laser profiler, an improved position calibration method for the 3D laser profiler is proposed. The new position calibration method allows to quickly and efficiently obtain the relative transformation of the laser profiler LCS to the gantry machine TCS. Then, a new OMM method is proposed to evaluate the thermal influence on the large-span crossbeam of a gantry machine tool. Moreover, six thermal error terms can be obtained only by a single measurement, which greatly reduces the error measurement time. The contributions of this study are summarized as follows:

(1) A linear axis kinematic model with the thermal error of the beam of a 3-axis gantry machining center is established, and the thermal error terms are separated to solve the six thermal errors of the linear axis.

(2) The calibration method of the 3D laser profiler on the machine tool is improved, and the transformation matrix between the LCS of the 3D laser profiler and the TCS of the machine tool can be solved simply and accurately. It is also analyzed that the calibration error has little influence on the proposed thermal error solution method and can be ignored.

(3) A 3D laser profiler was used to scan the artifact during the cold and warm-up process of the machine tool. The relative changes of the scanned point cloud are obtained by the NDT-ICP registration algorithm. The six thermal errors of the Y-axis can be solved with only single measurement and without stopping the machine tool.

This work presents a fast solution for the evaluation of 6 thermal errors in linear axes of machine tools. In our future work, we will try to extend this method to thermal error measurement of rotating axis.

Acknowledgements

The authors gratefully acknowledge the financial support of the National Natural Science Foundation of China (No. 52075337), the State Key Laboratory of Mechanical System and Vibration (No. MSVZD202113) and the Shanghai Pujiang Program (No. 2020PJD024).

Reference

[1] Reddy T N, Shanmugaraj V, Vinod P, et al. Real-time thermal error compensation strategy for precision machine tools[J]. Materials Today: Proceedings, 2020, 22: 2386-2396.

[2] Mayr J, Jedrzejewski J, Uhlmann E, et al. Thermal issues in machine tools[J]. CIRP annals, 2012, 61(2): 771-791.

[3] Onishi S, Ibaraki S, Kato T, et al. A self-calibration scheme to monitor long-term changes in linear and rotary axis geometric errors[J]. Measurement, 2022, 196: 111183.

[4] Mareš M, Horejš O. Modelling of cutting process impact on machine tool thermal behaviour based on experimental data[J]. Procedia Cirp, 2017, 58: 152-157.

[5] Li T, Yuan J, Zhang Y, et al. Time-varying reliability prediction modeling of positioning accuracy influenced by frictional heat of ball-screw systems for CNC machine tools[J]. Precision Engineering, 2020, 64: 147-156.

[6] Pahk H, Lee S W. Thermal error measurement and real time compensation system for the CNC machine tools incorporating the spindle thermal error and the feed axis thermal error[J]. The International Journal of Advanced Manufacturing Technology, 2002, 20(7): 487-494.

[7] Jia G, Cao J, Zhang X, et al. Ambient temperature-induced thermal error modelling for a special CMM at the workshop level based on the integrated temperature regression method[J]. The International Journal of Advanced Manufacturing Technology, 2022, 121(9): 5767-5778.

[8] Li H, Zhang P, Deng M, et al. Thermally induced comprehensive error modeling and compensation for gantry machine tools with grating scale in large structure machining[J]. The International Journal of Advanced Manufacturing Technology, 2020, 107(3): 1367-1376.
[9] Fu G, Zhou L, Zheng Y, et al. Improved unscented Kalman filter algorithm-based rapid identification of thermal errors of machine tool spindle for shortening thermal equilibrium time[J]. Measurement, 2022, 195: 111121.
[10] Liu J, Ma C, Wang S. Data-driven thermally-induced error compensation method of high-speed and precision five-axis machine tools[J]. Mechanical Systems and Signal Processing, 2020, 138: 106538.
[11] Gomez-Acedo E, Olarra A, Orive J, et al. Methodology for the design of a thermal distortion compensation for large machine tools based in state-space representation with Kalman filter[J]. International Journal of Machine Tools and Manufacture, 2013, 75: 100-108.
[12] Sato R, Shirase K. Geometric error compensation of five-axis machining centers based on on-machine workpiece measurement[J]. International Journal of Automation Technology, 2018, 12(2): 230-237.
[13] Abdulshahed A M, Longstaff A P, Fletcher S, et al. Thermal error modelling of a gantry-type 5-axis machine tool using a grey neural network model[J]. Journal of Manufacturing Systems, 2016, 41: 130-142.
[14] Ye W H, Guo Y X, Zhou H F, et al. Thermal error regression modeling of the real-time deformation coefficient of the moving shaft of a gantry milling machine[J]. Advances in Manufacturing, 2020, 8(1): 119-132.
[15] Ibaraki S, Blaser P, Shimoike M, et al. Measurement of thermal influence on a two-dimensional motion trajectory using a tracking interferometer[J]. CIRP annals, 2016, 65(1): 483-486.
[16] Mori M, Irino N, Shimoike M. A new measurement method for machine tool thermal deformation on a two-dimensional trajectory using a tracking interferometer[J]. CIRP annals, 2019, 68(1): 551-554.
[17] Ibaraki S, Inui H, Hong C, et al. On-machine identification of rotary axis location errors under thermal influence by spindle rotation[J]. Precision Engineering, 2019, 55: 42-47.
[18] Liu K, Liu H, Li T, et al. Intelligentization of machine tools: comprehensive thermal error compensation of machine-workpiece system[J]. The International Journal of Advanced Manufacturing Technology, 2019, 102(9): 3865-3877.
[19] Huang N, Zhang Y, Zhu L, et al. Visually quantifiable test piece for five-axis machine tools thermal effects[J]. Journal of Manufacturing Science and Engineering, 2022, 144(5).
[20] Ibaraki S, Okumura R. A machining test to evaluate thermal influence on the kinematics of a five-axis machine tool[J]. International Journal of Machine Tools and Manufacture, 2021, 163: 103702.
[21] Wiessner M, Blaser P, Böhl S, et al. Thermal test piece for 5-axis machine tools[J]. Precision Engineering, 2018, 52: 407-417.
[22] Zhao Z, Ding D, Fu Y. Error identification and compensation for a laser displacement sensor based on on-machine measurement[J]. Optik, 2021, 225: 165902.
[23] Ye J, Stewart E, Zhang D, et al. Method for automatic railway track surface defect classification and evaluation using a laser‐based 3D model[J]. IET Image Processing, 2020, 14(12): 2701-2710.
[24] ISO 230-1:2012(E), Test code for machine tools – Part 1: Geometric accuracy of machines operating under no-load or quasi-static conditions, 2012.
[25] ISO 230-3:2020(E), Test code for machine tools – Part 3: Determination of thermal effects, 2020.
[26] Zeng C, Hu Y, Shi J, et al. On-machine Measurement and Compensation of Assembling Gap for 5-axis Friction Stir Welding based on 2D Laser Profilometer[C]//2019 IEEE 5th International Conference on Mechatronics System and Robots (ICMSR). IEEE, 2019: 70-75.
[27] Powell M J D. A Fortran subroutine for solving systems of nonlinear algebraic equations[R]. Atomic Energy Research Establishment, Harwell, England (United Kingdom), 1968.
[28] Besl P J, McKay N D. Method for registration of 3-D shapes[C]//Sensor fusion IV: control paradigms and data structures. Spie, 1992, 1611: 586-606.
[29] Rusu R B, Marton Z C, Blodow N, et al. Towards 3D point cloud based object maps for household environments[J]. Robotics and Autonomous Systems, 2008, 56(11): 927-941.
[30] Magnusson M, Nuchter A, Lorken C, et al. Evaluation of 3D registration reliability and speed-A comparison of ICP and NDT[C]//2009 IEEE International Conference on Robotics and Automation. IEEE, 2009: 3907-3912.
[31] 2D/3D Laser Profiler: LJ-X8000 Series; Keyence: Shanghai, CN, 2022; Available online: https://www.keyence.com.cn/support/user/lj-x8000a/ (accessed on 26 August 2022).